Journal of ELECTRONIC MATERIALS
https://doi.org/10.1007/s11664-018-6126-8
© 2018 The Minerals, Metals & Materials Society

Nature of Dielectric Properties, Electric Modulus and AC Electrical Conductivity of Nanocrystalline $ZnIn_2Se_4$ Thin Films

M.M. EL-NAHASS,[1] A.A. ATTIA,[1] H.A.M. ALI,[1,2] G.F. SALEM,[1] and M.I. ISMAIL[1]

1.—Physics Department, Faculty of Education, Ain Shams University, Roxy, Cairo 11757, Egypt.
2.—e-mail: hend2061@yahoo.com

The structural characteristics of thermally deposited $ZnIn_2Se_4$ thin films were indexed utilizing x-ray diffraction as well as scanning electron microscopy techniques. Dielectric properties, electric modulus and AC electrical conductivity of $ZnIn_2Se_4$ thin films were examined in the frequency range from 42 Hz to 10^6 Hz. The capacitance, conductance and impedance were measured at different temperatures. The dielectric constant and dielectric loss decrease with an increase in frequency. The maximum barrier height was determined from the analysis of the dielectric loss depending on the Giuntini model. The real part of the electric modulus revealed a constant maximum value at higher frequencies and the imaginary part of the electric modulus was characterized by the appearance of dielectric relaxation peaks. The AC electrical conductivity obeyed the Jonscher universal power law. Correlated barrier hopping model was the appropriate mechanism for AC conduction in $ZnIn_2Se_4$ thin films. Estimation of the density of states at the Fermi level and activation energy, for AC conduction, was carried out based on the temperature dependence of AC electrical conductivity.

Key words: Nanocrystalline $ZnIn_2Se_4$, dielectric properties, electric modulus, electrical conductivity

INTRODUCTION

Chalcogenide materials have been extensively investigated for use in phase-change memory devices, and are regarded as highly promising candidates for next-generation nonvolatile memory.[1,2] They have received considerable attention over the past two decades due to their technological applications as electronic, optoelectronic and optical devices.[3–5]

$ZnIn_2Se_4$ is a ternary semiconductor that crystallizes in the uniaxial defect chalcopyrite structure of the S2/4 space group.[6,7] $ZnIn_2Se_4$ has a relatively high photoelectric sensitivity in the spectrum range from visible to near infrared, and it is predicted as being a promising material for optoelectronic applications.[7–10] In $ZnIn_2Se_4$ some percentage of 'Zn' vacancy sites cause disorder, which reveals a great number of electronic levels in the energy band gap region. This disorder produces some interesting optical and photoconductivity properties, which has led to the utilization of this material in varied fields such as photo-electronics and photovoltaics devices.[11] Some studies have investigated a portion of the properties for $ZnIn_2Se_4$ thin films. The study reported by El-Nahass et al.[12] demonstrated that $ZnIn_2Se_4$ thin films deposited at room temperature have a nanocrystalline structure with a crystallite size of a few nanometers. Moreover, the absorption analysis of the as-deposited $ZnIn_2Se_4$ films revealed the presence of allowed direct and indirect transitions. Dhruv et al.[6] studied the switching phenomenon in amorphous $ZnIn_2Se_4$ thin films as well as the parameters affecting the switching voltage. The investigation for the frequency and temperature reliance of AC conductivity, dielectric property, relaxation behavior of chalcogenide materials is

(Received October 15, 2017; accepted February 6, 2018)

Published online: 21 February 2018

widely used to understand the transport mechanism of charge carriers.[13]

The present work plans to study the electrical characteristics and dielectric properties of thermally evaporated $ZnIn_2Se_4$ thin films to provide useful information about the suitable conduction mechanism. Estimation of the dielectric constant, dielectric loss, electric modulus and AC electrical conductivity is performed in the frequency range of 42–10^6 Hz at different temperatures.

EXPERIMENTAL DETAILS

A $ZnIn_2Se_4$ ingot was prepared by the fusion of stoichiometric quantities of pure elements in vacuum-sealed silica tubes, which were left at 1323 K for 10 h and then cooled to room temperature over 48 h. Thin films of $ZnIn_2Se_4$ were deposited onto pre-cleaned glass substrates by thermal evaporation under a vacuum of about 10^{-4} Pa, at a deposition rate of 2 nm/s. The film was deposited at room temperature. The x-ray diffraction (XRD) pattern for the films was obtained using a Philips x-ray diffractometer with Cu(k_α) radiation (λ = 1.5418 Å). The surface morphology of the $ZnIn_2Se_4$ thin films was investigated using a scanning electron microscope (SEM Model Quanta 250 FEG, Field Emission Gun, FEI company, Netherlands). The dielectric measurements of the $ZnIn_2Se_4$ thin films were performed using a programmable automatic LCR bridge (model Hioki 3532 HiTester). $ZnIn_2Se_4$ films were sandwiched between two aluminum electrodes as an Al/$ZnIn_2Se_4$/Al structure. Measurements of capacitance C, conductance G and impedance Z were recorded in the frequency range 42–10^6 Hz at various temperatures. The temperature of the sample was checked using a thermocouple of chromel/alumel in the temperature range of 303–363 K. The total conductivity σ_{TOT} was determined from the relation: $\sigma_{TOT} = d/ZA_o$ where d is the thickness of the $ZnIn_2Se_4$ film and A_o is the cross-sectional area.

RESULTS AND DISCUSSION

Structure Analysis and Complex Permittivity

Figure 1 represents the XRD pattern for $ZnIn_2Se_4$ thin film of thickness 473 nm. The pattern shows a diffraction line at $2\theta°$ = 26.93° and a broad hump around $2\theta°$ = 46.57°. The Miller indices (hkl) of the planes are indexed utilizing (JCPDS card 80-0424). Hence, $ZnIn_2Se_4$ film has a nanocrystalline nature with a preferred orientation along the (112) plane of the tetragonal structure.[12] The surface morphology of $ZnIn_2Se_4$ thin film was investigated using scanning electron microscopy (SEM) techniques. Figure 2 displays a SEM image for $ZnIn_2Se_4$ film of thickness 473 nm. The surface of the film revealed spherically shaped particles distributed over the surface of $ZnIn_2Se_4$ in a homogenous nature with an average particle size of 20 nm.

The complex permittivity ε^* of semiconductors is given by $\varepsilon^* = \varepsilon_1 - j\varepsilon_2$. The real part of the permittivity, ε_1, is a measure of how much energy from an external electric field is stored in a material. The imaginary part of permittivity, ε_2, represents the loss of energy in a dielectric material occurring due to an external AC field. ε_1 and ε_2 are called dielectric constant and dielectric loss, respectively.[14] For $ZnIn_2Se_4$ thin film, ε_1 and ε_2 are determined in the frequency range 42–10^6 Hz using the relations[15]:

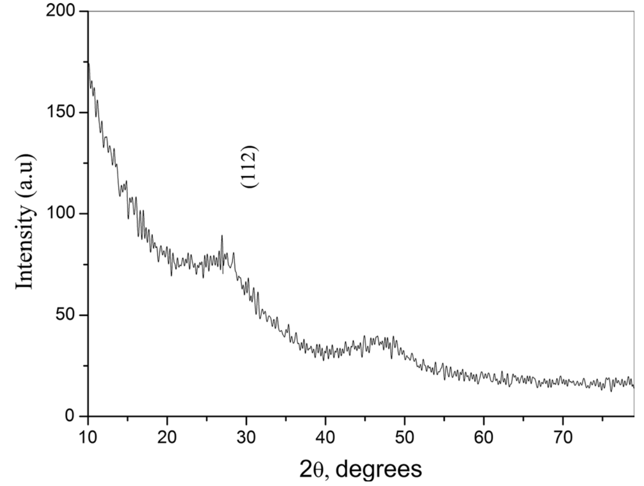

Fig. 1. XRD pattern of $ZnIn_2Se_4$ thin film of thickness 473 nm.

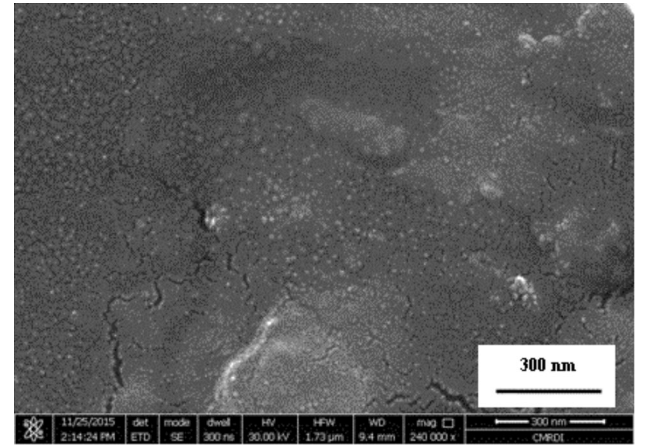

Fig. 2. SEM image of $ZnIn_2Se_4$ thin film of thickness 473 nm.

$$\varepsilon_1 = \frac{Cd}{\varepsilon_0 A_0} \quad (1)$$

$$\varepsilon_2 = \frac{Gd}{\varepsilon_0 A_0 \omega} \quad (2)$$

where ε_0 is the free space permittivity and ω (= $2\pi f$) is the angular frequency. Figure 3a represents the variation in dielectric constant ε_1 of $ZnIn_2Se_4$ thin film as a function of frequency at different temperatures. ε_1 (ω) decreases as the frequency increases. It decreased drastically in low-frequency and high-

temperature regions. This behavior indicates that electrode polarization and space charge effects have occurred, confirming the non-Debye dependence.[16,17] At high frequencies, the dipoles cannot rotate themselves upon the increase in the field, and thus there is a weak dependence of ε_1 (ω) on frequency. Moreover, ε_1 increases with the increase in temperature at a certain value of frequency, as seen in Fig. 3b. It may be due to space charge polarization that the charge carriers are not free to move, but they are trapped, causing polarization. By increasing the temperature, the number of charge carriers increases, producing further space charge polarization and leading to a rapid increase in the dielectric constant ε_1.[18]

Figure 4a, b shows the variation in dielectric loss ε_2 of $ZnIn_2Se_4$ thin film as a function of frequency and temperature, respectively. The value of ε_2 decreases with the increase in frequency, and increases with temperature. The dielectric loss of a material can be divided into three parts: conduction losses, dipole losses and vibrational losses.[19] The conduction loss occurs because of migration of ions over large distances. When the ions move, they give some of their energy to the lattice as heat. It is lower at low temperatures because it is proportional to the ratio of $\sigma_{AC}(\omega)/\omega$, where σ_{AC} is the AC conductivity. As $\sigma_{AC}(\omega)$ increases with increase in temperature, the conduction loss increases.[20]

The behavior of ε_2 as a function of both frequency and temperature can be analyzed according to the model described by Giuntini et al.[21–23] In this model, the imaginary part of the dielectric constant is expressed as:

$$\varepsilon_2(\omega) = (\varepsilon_s - \varepsilon_\infty)2\pi^2 N\left(\frac{ne}{\varepsilon_s}\right)^3 kT\tau_0^m W_m^{-4}\omega^m \quad (3)$$

where ε_s is the static dielectric constant, ε_∞ is dielectric constant at infinitely high frequencies, n is the number of electrons that hop, e is the electronic charge, N is concentration of localized states, T is the absolute temperature, k is the Boltzmann constant, τ_0 is the characteristic relaxation time, W_m is the energy required to move the electron from one site to infinity, maximum barrier

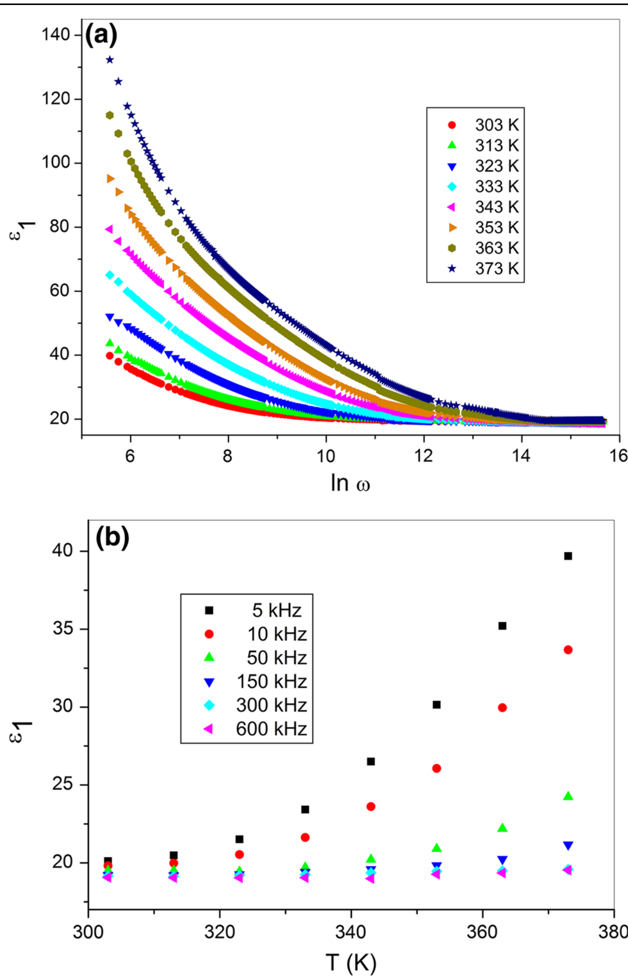

Fig. 3. Dielectric constant ε_1, as a function of (a) frequency and (b) temperature for $ZnIn_2Se_4$ thin film.

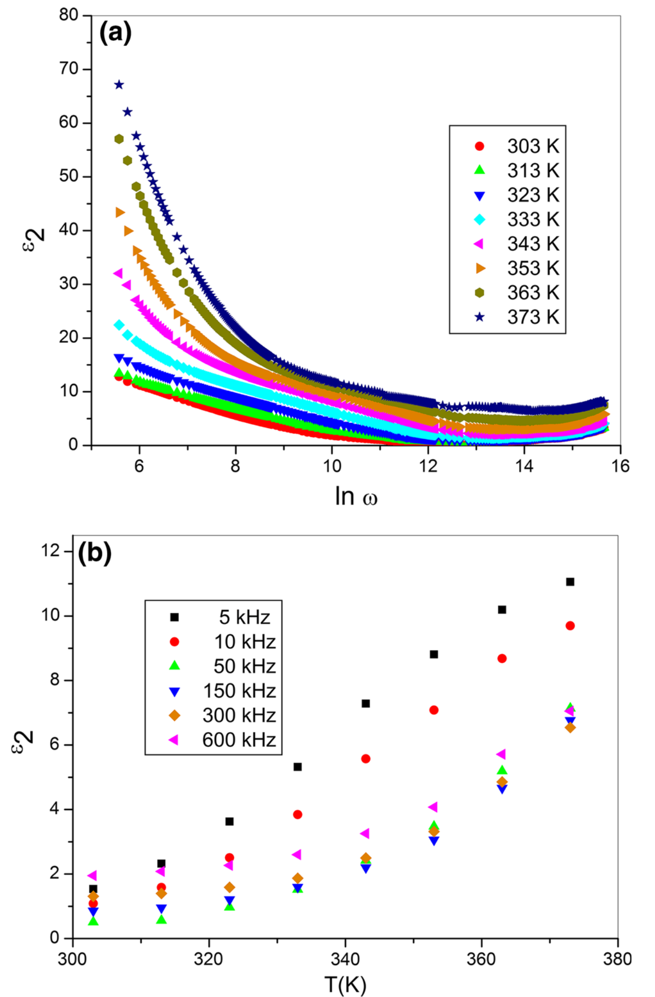

Fig. 4. Dielectric loss ε_2, as a function of (a) frequency and (b) temperature for $ZnIn_2Se_4$ thin film.

height, and m is a power of angular frequency (ω) and is given by[24]:

$$m = \frac{-4kT}{W_m} \quad (4)$$

The variation in ε_2 with the angular frequency according to Eq. (3) can be written as a power law[25] as:

$$\varepsilon_2 = B\omega^m \quad (5)$$

where B is a constant. The values of m were calculated in the frequency range of 42–6×10^4 Hz as a function of temperature, by plotting $\ln \varepsilon_2$ versus $\ln \omega$, as can be seen in Fig. 5a. It is found that m decreases with the increase of temperature in Fig. 5b. The fitting of the data of m gives a linear relation. The value of W_m was determined from the slope of this relation and found to be 0.4 eV. The value of W_m is also identified in terms of the optical band gap (E_g), where $W_m = E_g/4$.[26] E_g of $ZnIn_2Se_4$ thin films is obtained by El-Nahass et al.,[12] which has a value of 1.71 eV. Thus, the expected value of W_m is 0.43 eV. This value shows good agreement with that proposed from the Giuntini model.

Real and Imaginary Parts of the Electric Modulus

The electric modulus, M^*, can be used to understand electrical relaxation processes. It corresponds to the relaxation of the electric field in the material when the electric displacement remains constant and is defined as the reciprocal of the complex permittivity (ε^*)[27] as:

$$M^* = \frac{1}{\varepsilon^*} = M_1 + jM_2 \quad (6)$$

The real (M_1) and imaginary (M_2) parts of M^* are given as:

$$M_1 = \frac{\varepsilon_1}{\varepsilon_1^2 + \varepsilon_2^2} \quad (7)$$

$$M_2 = \frac{\varepsilon_2}{\varepsilon_1^2 + \varepsilon_2^2} \quad (8)$$

The frequency dependence of M_1 and M_2 for $ZnIn_2Se_4$ thin film at various temperatures is shown in Figs. 6 and 7, respectively. The real part of the electric modulus shows an increase in its value as the frequency increase for the different temperatures. Further, M_1 saturates at a maximum value at high frequencies for each temperature, indicating a relaxation process[28] in $ZnIn_2Se_4$. Also, at a certain value of frequency, M_1 decreases with the rise in temperature. The imaginary part of $ZnIn_2Se_4$, Fig. 7, increases with the increase in frequency reaching a maximum value $(M_2)_{max}$ then decreases for the different temperatures. For frequencies below the maximum value, the charge carriers are mobile over long distances. At frequencies above the maximum value, the carriers are to be confined to the potential well. Thus, the carriers are mobile over a short distance.[29,30]

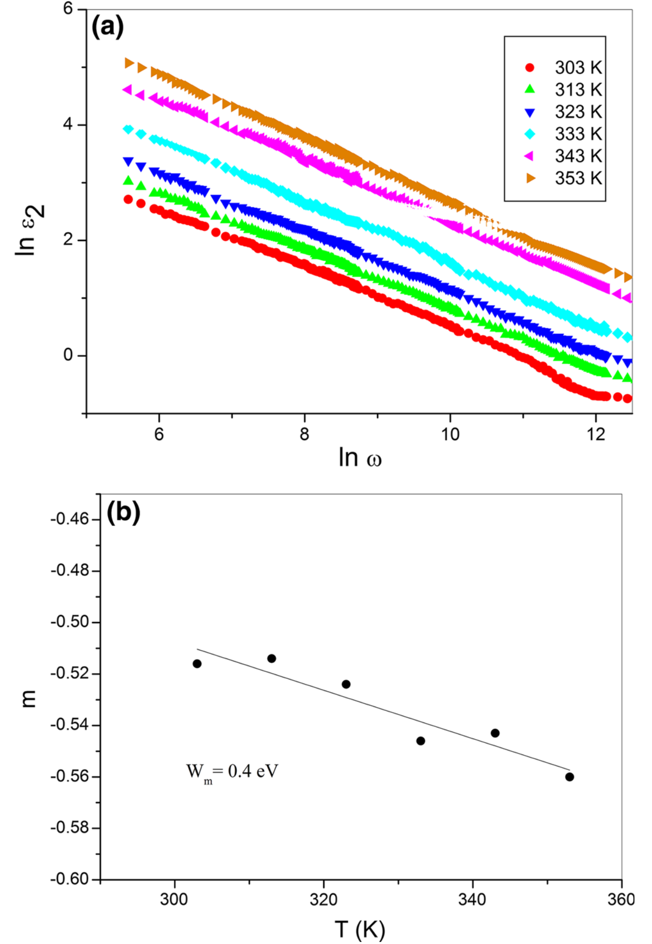

Fig. 5. (a) Plot of $\ln \varepsilon_2$ versus $\ln \omega$ and (b) temperature dependence of m for $ZnIn_2Se_4$ thin film.

The position of $(M_2)_{max}$ on the frequency axis corresponds to the relaxation peak and it shifts to higher frequencies with increasing temperature. The frequency ω_m gives the most probable relaxation time τ from the condition $(\omega_m \cdot \tau) = 1$. The relaxation time of $ZnIn_2Se_4$ thin film follows the Arrhenius law expressed by the relation[31,32]:

$$\tau = \tau_c exp\left(\frac{\Delta E_a}{kT}\right) \quad (9)$$

where τ_c is the pre-exponential factor and ΔE_a is the activation energy of the relaxation process. Figure 8 shows the temperature dependence of relaxation time as a linear relation. The activation energy ΔE_a was found to be 0.73 eV.

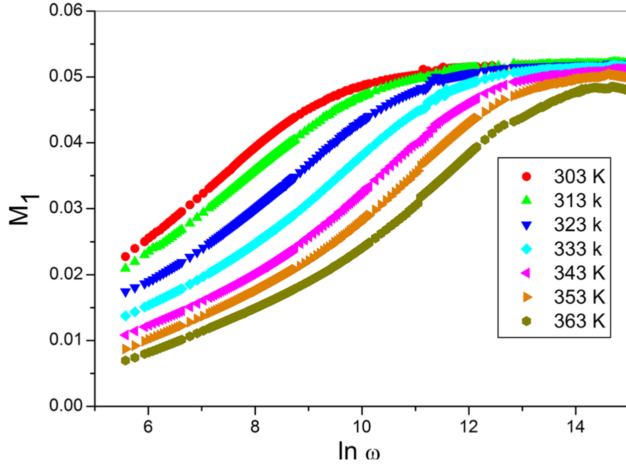

Fig. 6. Real part of electric modulus M_1 as a function of frequency for $ZnIn_2Se_4$ thin film.

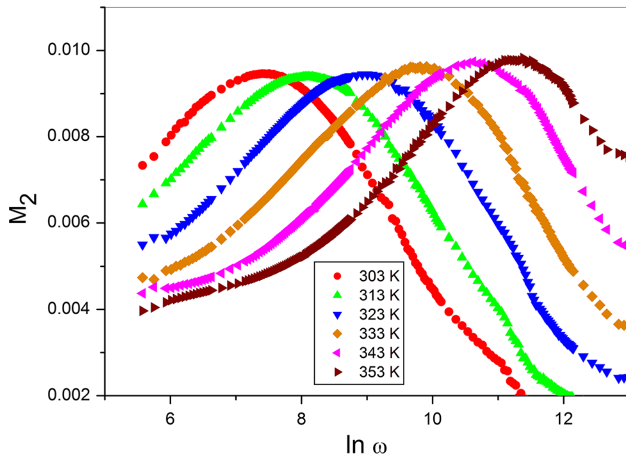

Fig. 7. Imaginary part of electric modulus M_2 as a function of frequency for $ZnIn_2Se_4$ thin film.

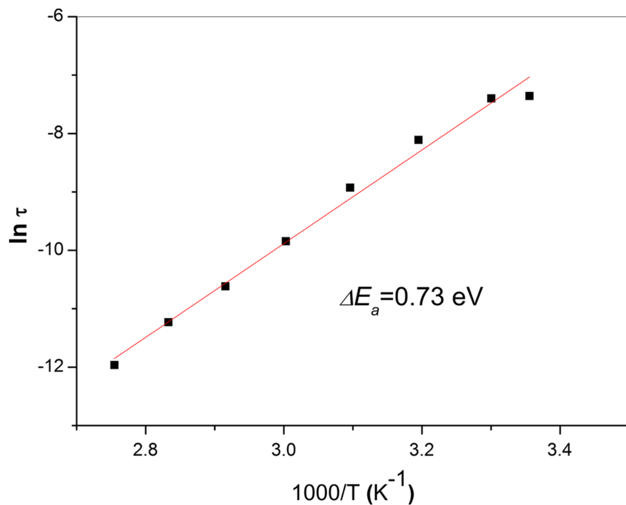

Fig. 8. Temperature dependence of relaxation time τ for $ZnIn_2Se_4$ thin film.

AC Conductivity

The AC electrical conductivity σ_{AC} (ω), for $ZnIn_2Se_4$ thin film of thickness 473 nm measured in the frequency range 42–10^6 Hz. σ_{AC} (ω) is calculated using the relation[33]: $\sigma_{AC}(\omega) = \sigma_{TOT} - \sigma_{DC}$, where σ_{DC} is the frequency-independent conductivity and it is the value of σ_{TOT} at low frequency down to zero.[34] Figure 9 shows the variation in σ_{AC} as a function of frequency for $ZnIn_2Se_4$ film at different temperatures. From the figure, σ_{AC} increases linearly with increasing frequency according to the Jonscher power law[35,36] as:

$$\sigma_{AC}(\omega) = A\omega^s \tag{10}$$

where A is a constant and s is the frequency exponent, generally less than unity. Different theories have been developed to explain the frequency dependence of the AC conductivity of semiconductors. Two fundamental theories[37] have been developed to account for the frequency dependence of σ_{AC} data. They are the quantum mechanical tunneling mechanism proposed by Pollak and Geballe[38] and the hopping over barrier mechanism proposed by Pike[39] and Elliott.[40] To explain the σ_{AC} data and the applicable mechanism for the AC conduction in $ZnIn_2Se_4$, the temperature-dependent behavior of the frequency exponent is investigated. Values of s are calculated from the slope of plotting ln σ_{AC} versus ln ω (Fig. 9) for the different temperatures. The dependence of the frequency exponent on temperature is displayed in Fig. 10. It is clear that the frequency exponent decreases with the increase in temperature. This behavior confirms that correlated barrier hopping (CBH) model is the dominant current transport mechanism for $ZnIn_2Se_4$. In the CBH model, the AC conductivity is given by[41]:

$$\sigma_{AC}(\omega) = \left(\frac{\pi}{3}\right)[N(E_F)]^2 kTe^2\alpha^{-5}\omega\left[ln\left(\frac{\nu_p}{\omega}\right)\right]^4 \tag{11}$$

where $N(E_F)$ is the density of localized states near the Fermi level, α is the exponential decay parameter of localized states wave functions and ν_p is the frequency of the phonons. Taking ν_p of 10^{12} Hz and α^{-1} of 10 Å,[24] $N(E_F)$ is determined at different frequencies for $T = 303$ K. It is observed from Fig. 11 that $N(E_F)$ values increase with the increase in the frequency.

Figure 12 shows the temperature dependence of AC electrical conductivity for $ZnIn_2Se_4$ thin film at different frequencies. It is seen from the figure that σ_{AC} is increased with increasing temperature as observed for several semiconductors. The temperature dependence of σ_{AC} obeys the well-known Arrhenius relation[24]:

$$\sigma_{AC} = \sigma_0 e^{\frac{-\Delta E}{kT}} \tag{12}$$

where σ_o is a constant and ΔE is the activation energy for AC conduction in $ZnIn_2Se_4$ thin film. The activation energy was estimated from the slope of ln

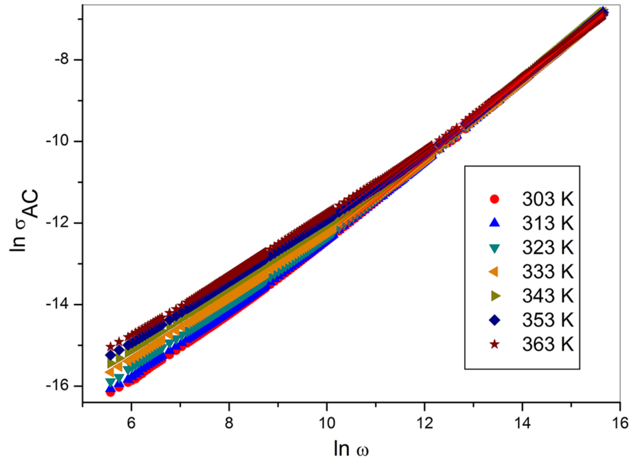

Fig. 9. The AC conductivity σ_{AC}, of $ZnIn_2Se_4$ as a function of frequency at different temperatures.

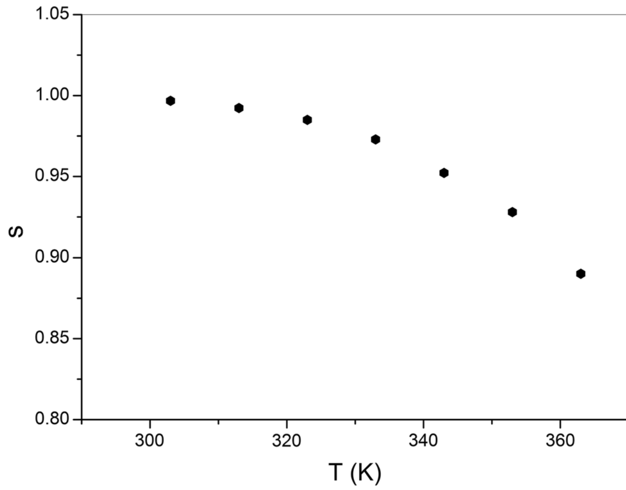

Fig. 10. Temperature dependence of frequency exponent s for $ZnIn_2Se_4$ thin film.

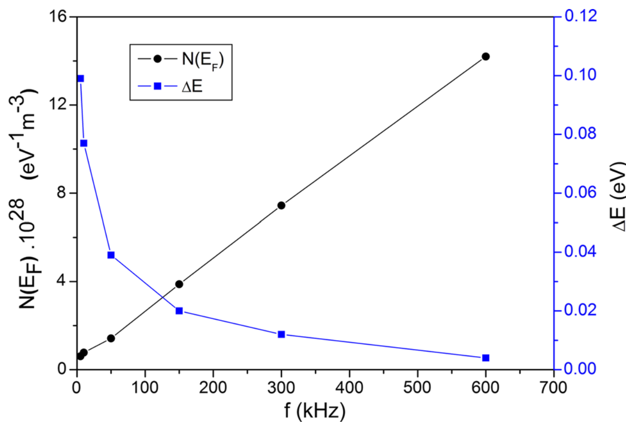

Fig. 11. Frequency dependence of $N(E_F)$ and ΔE for $ZnIn_2Se_4$ thin film.

σ_{AC} versus $1000/T$ plots at different frequencies. The frequency dependence of the activation energy is shown in Fig. 11. As seen, ΔE diminishes with the increase of frequency that is consistent with behavior observed for bulk $ZnIn_2Se_4$.[24] This result verifies the mechanism of correlated barrier hopping for AC conduction. The increased applied field frequency enhances electronic jumps between localized states. Consequently, the AC activation energy decreases with increasing frequency.[42]

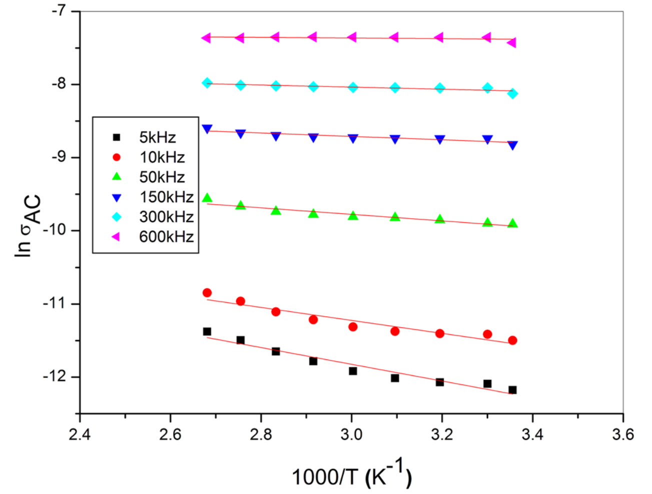

Fig. 12. The AC electrical conductivity σ_{AC} of $ZnIn_2Se_4$ thin film as a function of temperature at different frequencies.

CONCLUSION

The XRD pattern of thermally deposited $ZnIn_2Se_4$ thin film shows that the film has a nanocrystalline structure with a preferred orientation along the (112) plane. The SEM image for $ZnIn_2Se_4$ film reveals a homogeneous distribution of spherical particles with an average size of 20 nm. The dielectric constant and dielectric loss of $ZnIn_2Se_4$ thin film decreased with the rise in frequency and increased with increasing temperature. The maximum barrier height W_m was determined according to Giuntini model and found to be 0.4 eV. The real part of the electric modulus revealed a saturated maximum value at higher frequencies. Dielectric relaxation peaks in the imaginary part of the electric modulus spectra shifted to higher frequencies with increasing temperature. Arrhenius behavior was observed for the dielectric relaxation times. The AC conductivity of $ZnIn_2Se_4$ thin film obeys the Jonscher universal power law. The CBH model is the predominant current transport mechanism for AC conduction. The AC conductivity increased with increasing temperature at different frequencies. The activation energy ΔE decreased with the increase in frequency.

REFERENCES

1. I.H. Khudayer, *Int. J. Curr. Eng. Technol.* 4, 495 (2014).
2. D.S. Jeong, G.-H. Park, H. Lim, C.S. Hwang, S. Lee, and B.-K. Cheong, *Appl. Phys. A* 102, 1027 (2011).
3. N.A. Hegab and H.M. El-Mallah, *Acta Phys. Pol. A* 116, 1048 (2009).

4. M.M. Hafiz, N. El-Kabany, H. Kotb, and Y.M. Mahfoz Bakier, *Int. J. Thin. Fil. Sci. Tec.* 4, 163 (2015).
5. A.S. Faidah, *Chalcogenide Lett.* 5, 359 (2008).
6. D.K. Dhruv, A. Nowicki, B.H. Patel, and V.D. Dhamecha, *Surf. Eng.* 31, 556 (2015).
7. P. Babu, M.V. Reddy, N. Revathi, and K.T.R. Reddy, *J. Nano- Electron. Phys.* 3, 85 (2011).
8. G. Alagumuthu and T. Anantha Kumar, *Nanosci. Nanotechnol. An Int. J.* 5, 41 (2015).
9. D.K. Dhruv and B.H. Patel, *Int. J. Adv. Res. Electr. Electron. Instrum.* 3, 9 (2015).
10. D.K. Dhruv and B.H. Patel, *Mater. Sci. Semicond. Process.* 54, 29 (2016).
11. P. Babu, M.R.V. Reddy, and K.T.R. Reddy, *Electron. Mater. Lett.* 10, 731 (2014).
12. M.M. El-Nahass, A.A. Attia, G.F. Salem, H.A.M. Ali, and M.I. Ismail, *Physica B Physica B* 425, 23 (2013).
13. M. Haj Lakhdar, B. Ouni, and M. Amlouk, *Mater. Sci. Semicond. Process.* 19, 32 (2014).
14. H. Kassem, V. Vigneras, and G. Lunet, *Microwave and millimeter wave technologies: from photonic bandgap devices to antenna and applications*, ed. I. Minin (Croatia: InTeh, 2010), p. 289.
15. A. Tataroglu, *GU J. Sci.* 26, 501 (2013).
16. X. Qian, N. Gu, Z. Cheng, X. Yang, E. Wang, and S. Dong, *Electrochim. Acta* 46, 1829 (2001).
17. A.S. ELmezayyen and M. Fikry, *Reicha, Open Journal of Applied Sciences* 5, 415 (2015).
18. T. Tunc, I. Uslu, I. Dokme, S. Altındal, and H. Uslu, *Int. J. Polymer. Mater.* 59, 739 (2010).
19. T. Mathew, A.G. Kunjomana, K. Munirathnam, K.A. Chandrasekharan, M. Meena, and C.K. Mahadevan, *Cryst. Struct. Theory. Appl.* 1, 79 (2012).
20. A. Kumar, M. Lal, K. Sharma, and N. Goyal, *J. Non-Oxide Glasses* 5, 47 (2013).
21. J.C. Giuntini, J.V. Zanchetta, D. Jullien, R. Eholie, and P.J. Houenou, *Non-Cryst. Solids* 45, 57 (1981).
22. M.M. El-Nahass, H. Kamal, M.H. Elshorbagy, and K. Abdel-Hady, *Org. Electron.* 14, 2847 (2013).
23. A.M. Nawar, H.M. Abd El-Khalek, and M.M. El-Nahass, *Org. Opto-Elect.* 1, 25 (2015).
24. M.M. El-Nahass, A.A. Attia, G.F. Salem, H.A.M. Ali, and M.I. Ismail, *Phys. B* 434, 89 (2014).
25. M.A.M. Seyam, A.E. Bekheet, and A. Elfalaky, *Eur. Phys. J. Appl. Phys.* 16, 99 (2001).
26. A.E. Bekheet and N.A. Hegab, *Vacuum* 83, 391 (2009).
27. N.D. Sankır, E. Aydın, and M. Sankır, *Int. J. Electrochem. Sci.* 9, 3864 (2014).
28. L. Patro and K. Hariharan, *Mater. Chem. Phys.* 116, 81 (2009).
29. A. Mogugs-Milankovic, A. Santic, V. Licina, D.E. Day, and J. Non-Cryst, *Solids* 351, 3235 (2005).
30. A.A.A. Darwish, M.M. El-Nahass, and A.E. Bekheet, *J. Alloys Compd.* 586, 142 (2014).
31. R.M.-L. Kitaneh, M.M. Abu-Samreh, S.M. Musameh, S.M. Hraibat, and A.M. Saleh, *Appl. Phys. A* 114, 1267 (2014).
32. S. Kumar, M. Husain, and M. Zulfequar, *Phys. B* 387, 400 (2007).
33. A.E. Bekheet, *Phys. B* 403, 4342 (2008).
34. M.M. El-Nahass and H.A.M. Ali, *Solid State Commun.* 152, 1084 (2012).
35. N.F. Mott and E.A. Davis, *Electronic Processes in Non-Crystalline Materials*, 2nd ed. (New York, Oxford: Clarendon Press, 1979).
36. A.M. Badr, H.A. Elshaikh, and I.M. Ashraf, *J. Eng. Technol. Res.* 3, 62 (2011).
37. R.A.H. El-Mallawany, *Tellurite Glasses Handbook: Physical Properties and Data, 2nd end* (Boca Raton: CRC Press, 2011).
38. M. Pollak and T.H. Geballe, *Phys. Rev.* 122, 1742 (1961).
39. G.E. Pike, *Phys. Rev B* 6, 1572 (1972).
40. S.R. Elliott, *Phlios. Mag.* 36, 1291 (1977).
41. I.G. Austin and N.F. Mott, *Adv. Phys.* 18, 41 (1969).
42. M.M.H. Khalil and O.A. Desouky, *Int. J. Adv. Res.* 2, 598 (2014).